Fungal Biology 129 (2025) 101561

Contents lists available at ScienceDirect

Fungal Biology

journal homepage: www.elsevier.com/locate/funbio

Metabolomic profiles of the infection pathways of *Calcarisporium cordycipiticola* on the cultivated and medicinal mushroom, *Cordyceps militaris*

Li Lu [a,b,c,d,e], Mahesh C.A. Galappaththi [f], Nimesha M. Patabendige [g], Yu-Zhe Feng [a], Tian Yang [a], Samantha C. Karunarathna [e], Jiang-Tao Xie [a], Eleni Gentekaki [d], Sylvie Rapior [h,i], Esteban Charria-Girón [j,k], Marc Stadler [j,k], Wei-Feng Ding [l,m], Feng-Hua Tian [a,b], Xiang-Yu Zeng [a,b,c,*]

[a] *Department of Plant Pathology, College of Agriculture, Guizhou University, Guiyang, 550025, PR China*
[b] *Institute of Edible Mushrooms, Guizhou University, Guiyang, 550025, PR China*
[c] *Center of Excellence in Fungal Research, Mae Fah Luang University, Chiangrai,57100, Thailand*
[d] *School of Science, Mae Fah Luang University, Chiangrai, 57100, Thailand*
[e] *Center for Yunnan Plateau Biological Resources Protection and Utilization, Key Laboratory of Yunnan Provincial Department of Education of the Deep-Time Evolution on Biodiversity from the Origin of the Pearl River, College of Biology and Food Engineering, Qujing Normal University, Qujing, Yunnan 655011, PR China*
[f] *Harry Butler Institute, Murdoch University, Murdoch, WA 6150, Australia*
[g] *School of Medical, Molecular and Forensic Sciences, Murdoch University, Murdoch, WA 6150, Australia*
[h] *CEFE, Univ Montpellier, CNRS, EPHE, IRD, 15 Avenue Charles Flahault, cedex 5, 34093, Montpellier, France*
[i] *Laboratory of Botany, Phytochemistry and Mycology, Faculty of Pharmacy, University of Montpellier, CS 14491, 15 Avenue Charles Flahault, cedex 5, 34093, Montpellier, France*
[j] *Dept. Microbial Drugs, Helmholtz Centre for Infection Research, Inhoffenstrasse 7, 38124, Braunschweig, Germany*
[k] *Institute of Microbiology, Technische Universität Braunschweig, Spielmannstraße 7, 38106, Braunschweig, Germany*
[l] *Institute of Highland Forest Science, Chinese Academy of Forestry, Kunming, 650224, PR China*
[m] *Key Laboratory of Breeding and Utilization of Resource Insects, National Forestry and Grassland Administration, Kunming, 650224, PR China*

ARTICLE INFO

Handling Editor: Prof Han Wosten

Keywords:
Deleterious fungus–mushroom interaction
Mycotoxins
Secondary metabolites
White mildew disease

ABSTRACT

Cordyceps militaris is a widely cultivated mushroom with multiple medicinal properties. However, the emergence of white mildew disease caused by *Calcarisporium cordycipiticola* has become a serious dilemma, leading to economic losses in its industrial production. The genome of *Ca. cordycipiticola* possesses more secondary metabolite biosynthetic gene clusters and a smaller number of genes encoding for carbohydrate-active enzyme secretion than other mycoparasites. To uncover those functional metabolites correlated with the infection process, metabolomic profiles between healthy *C. militaris* fruit bodies (CK) and healthy (HFB) and diseased (DFB) parts of infected *C. militaris* fruit bodies by *Ca. cordicipiticola* were compared based on untargeted metabolomic analyses. The function of different metabolites during the pathogen infection and host response processes were further analyzed according to their respective metabolic pathways. Results of key metabolic pathway analyses suggested that a sterigmatocystin-like metabolite functions as one of the virulence factors of white mildew disease on *C. militaris*, whereas *S*-adenosyl-L-methionine represents a hub intermediate in both processes of pathogen infection and host response, highlighting the relevance of methyl group turnovers in this battle. More importantly, the detection of toxic metabolites in diseased *C. militaris* fruiting bodies suggests that this macrofungus contaminated by *Ca. cordycipiticola* should not be consumed due to the risk that it may contain related instead toxins. This study hypothesizes on the scenario of key metabolic biosynthesis in the battle between *Ca. cordycipiticola* and *C. militaris*. Our instead findings not only shed light on the interaction between the pathogen and the host but also provide crucial insights for the development of effective prevention and control strategies in the future.

* Corresponding author. Department of Plant Pathology, College of Agriculture, Guizhou University, Guiyang, 550025, PR China.
E-mail address: xyzeng3@gzu.edu.cn (X.-Y. Zeng).

https://doi.org/10.1016/j.funbio.2025.101561
Received 15 November 2024; Received in revised form 24 February 2025; Accepted 24 February 2025
Available online 26 February 2025

Abbreviations

AF	Aflatoxin
AFB1	Aflatoxin B1
ATP	Adenosine triphosphate
BGCs	Biosynthetic gene clusters
CAZymes	Carbohydrate-active enzymes
CK	Healthy fruiting bodies for control
DAD	Diode array detector
dSAM	*S*-adenosylmethioninamine
dU	2′-deoxyuridine
DFB	Diseased parts of infected fruiting bodies
DH	DFB vs HFB
DC	DFB vs CK
HC	HFB vs CK
HFB	Healthy parts of infected fruiting bodies
ESI	Electrospray ion source
FC	Fold change
HMT	Homocysteine *S*-methyltransferase
HPLC	High-performance liquid chromatography
Ins(1,3,4,5,6)P5	1D-myo-inositol 1,3,4,5,6-pentakisphosphate
Ins(3,4,5,6)P4	D-myo-inositol 3,4,5,6-tetrakisphosphate
KGDHC	α-Ketoglutarate dehydrogenase complex
LC	Liquid chromatography
LC-MS/MS	Liquid chromatography coupled with tandem mass spectrometry
m/z	Mass-to-charge ratio
Met	L-methionine
MS	Mass spectrometry
MTA	5′-methylthioadenosine
OPLS-DA	Orthogonal partial least squares-discriminant analysis
p	p-value
PCA	Principal component analysis
PLS-DA	Partial least squares-discriminant analysis
QC	Quality control
ROS	Reactive oxygen species
RT	Retention time
SAH	*S*-adenosyl-L-homocysteine
SAM	*S*-adenosyl-L-methionine
SIH	*S*-inosyl-L-homocysteine
SMM	*S*-methyl-L-methionine
ST	Sterigmatocystin
UTP	Uridine triphosphate
UV–Vis	Ultraviolet–visible
VIP	Variable importance in projection

1. Introduction

Calcarisporium cordycipiticola is a mycoparasite characterized by hyaline, erect, whorled conidiophores and sympodial conidiations, which has so far only been encountered on the fruiting bodies of *Cordyceps militaris* (Sun et al., 2016). After detecting the host, this pathogen first invades the hyphal interstices of the host in a biotrophic lifestyle while suppressing the host's immune response and then degrades the hyphal cells before starting a mode of saprobic life, which is the cause of downy mildew disease, representing a significant economic losses (Liu and Dong, 2023; Liu et al., 2021; Sun et al., 2016). The genome of *Ca. cordycipiticola* is similar in size to those of *Trichoderma* spp. mycoparasites but has a much smaller number of carbohydrate-active enzymes (CAZymes) than those of other mycoparasites, particularly those encoding cell wall-degrading proteins; it has a large number of biosynthetic gene clusters (BGCs), including those involved in mycotoxins production (Liu et al., 2021). This indicates the use of different infection strategies than other mycotrophic fungi, such as *Clonostachys* and *Trichoderma* species, which typically kill host fungi by secreting cell wall degrading enzymes (Karlsson et al., 2015), making *Ca. cordycipiticola* specifically infecting *C. militaris* (Liu et al., 2021).

Previous OMIC studies on *Ca. cordycipiticola* infecting *C. militaris* focused on genomic and transcriptomic analyses, while metabolomic studies have yet to be performed (Chen et al., 2019; Liu and Dong, 2023; Liu et al., 2021). Metabolomics focuses on the analysis of primary and secondary metabolites, end products of cellular regulatory processes, the levels of which can be considered the ultimate response of biological systems to various stressors and environmental changes (Fiehn, 2002; Matich et al., 2019). Fungicolous fungi generally possess a large number of BGCs, but most of them are silent under laboratory conditions (Cheng et al., 2021). There are 66 core BGCs of secondary metabolites identified in the genome of *Ca. cordycipiticola*, which is double the number found in its host, *C. militaris*. These include non-ribosomal peptide synthases (NRPSs), type I polyketide synthases (T1PKSs), NRPS-PKS hybrids, putative NRPS-like enzymes, indoles, and terpenes (Liu et al., 2021).

Comparison of these BGCs against the Minimum information about a biosynthetic gene cluster (MiBiG) database allowed the annotation of aureobasidin A1, botryenalol, clavaric acid, depudecin, dimethylcoprogen, phomopsins, and pyranonigrin E clusters (Liu et al., 2021). In addition, there were 66 BGCs of secondary metabolites being revealed in the genome of another mycoparasitic species of *Ca. arbuscula*, including gene clusters for aflatoxin (AF), alternariol, aurovertin, citrinin, destruxin, isoflavipucine, and other mycotoxins (Cheng et al., 2020). Nevertheless, there is still a lack of knowledge on the production of secondary metabolites produced by *Calcarisporium* species, especially those related to the pathogen-host interactions.

To uncover functional metabolites that correlate with the infection process of *Ca. cordycipiticola* and the host response, untargeted metabolomic analyses between healthy and diseased *C. militaris* fruiting bodies were conducted based on liquid chromatography coupled with tandem mass spectrometry (LC-MS/MS) . Secondary metabolites were then putatively identified and significantly differential mycotoxin-like metabolites were selected for further analyses. Their correlative metabolic pathways and function in pathogen infection and host response processes were systematically investigated. The presence of key virulence metabolites was further demonstrated using metabolic pathway analysis and BGC synteny analysis. This study investigated the steady-state end products of the deleterious fungus–mushroom interaction between *Ca. cordycipiticola* and *C. militaris*, which charts a more explicit picture of the entire infection process combining genomic and metabolomic data.

2. Materials and methods

2.1. Sample collections and preparation

Healthy and diseased fruiting bodies of three-month-old *C. militaris* were collected for this study (Fig. 1). They were divided into three groups each for future analyses, including healthy fruiting bodies for control (denotes as CK) with four replicates, healthy parts of infected fruiting bodies (denotes as HFB) with three replicates, and diseased parts of infected fruiting bodies (denotes as DFB) with three replicates. Each group was a mix of three different mushroom samples. The quality control (QC) sample was prepared by mixing samples from the above three groups.

Sixty milligrams of samples from each group were placed in a 2 mL centrifuge tube containing a 100 mg glass bead inside. One mL of a 50 % hydro-methanolic mixture (stored at 4 °C) was then added to the tube and vortexed for 30 s. After placing the tube in a 2 mL adapter matching

the instrument, it was immersed in the liquid nitrogen for 5 min. The mushroom sample was then ground using a tissue grinder at 55 Hz for 2 min, repeated twice. After freezing was completed, the tube was centrifuged at 12,000 rpm for 10 min, and its supernatant was transferred to a new centrifuge tube for concentration and drying. Finally, 300 μL of 2-chloro-L-phenylalanine solution (4 ppm) prepared with 50 % hydro-methanolic solution (stored at 4 °C) was added to dissolve the sample again, and then the supernatant was filtered by a 0.22 μm membrane in the detection bottle. All three groups (10 replicates) were analyzed using the LC-MS/MS system at PANOMIX Biomedical Tech Co., Ltd. (Shuzhou, China).

2.2. Global untargeted metabolomic analysis

Liquid chromatography (LC) analysis was performed on an Ultimate 3000 UHPLC System (Thermo Fisher Scientific, USA). Chromatography was carried out with an ACQUITY UPLC® HSS T3 (150 × 2.1 mm, 1.8 μm) (Waters, Milford, MA, USA). The column was maintained at 40 °C. The flow rate and injection volume were set at 0.25 mL/min and 2 μL, respectively. The mobile phases for positive ion mode consisted of 0.1 % (v/v) formic acid in a mixture of acetonitrile and water. For negative ion mode, the analysis was carried out with acetonitrile and ammonium formate (5 mM) in water. Separations were conducted under the following gradient of both mobile phases: 0–1 min at 2 %, 1–9 min from 2% to 50 %, 9–12 min from 50% to 98 %, 12–13.5 min at 98 %, 13.5–14 min from 98% to 2%, and 14–20 min at 2 %.

Mass spectrometric (MS) detection of metabolites was performed on the Q Exactive mass spectrometer (Thermo Fisher Scientific, USA) with an electrospray ion source (ESI). Full MS followed by data-dependent MS/MS mode was used with the following parameters: 3.50 kV and −2.50 kV spray voltage for ESI (+) and (−) respectively, 30 arb sheath gas pressure and 10 arb aux gas flow, 325 °C capillary temperature, 70000 and 17500 FWHM (full width at half maximum) resolving power for MS and MS/MS respectively, the mass-to-charge ratio (m/z) 81–1000 MS range, 10 data-dependent scans per cycle, 30 eV normalized collision energy, automatic dynamic exclusion time.

2.3. Data processing and multivariate statistical analysis

The raw data were firstly converted to mzXmL formatted by MSConvert in ProteoWizard software package (v3.0.8789) and processed using XCMS package in R software for feature detection, RT correction and alignment (ppm = 15, peakwidth = c(5, 30), mzdiff = 0.01, method = centWave). Missing values were imputed with k nearest neighbors (KNN) algorithm ($k = 10$, distance = Euclidean) (Troyanskaya et al., 2001). The quality control–based robust LOESS (locally estimated scatterplot smoothing) signal correction (QC-RLSC) was applied for data normalization to correct for any systematic bias (Dunn et al., 2011). After normalization, only ion peaks with relative standard deviations (RSDs) less than 30 % in QC were kept to ensure proper metabolite identification.

Data were mean-centered using scaling before multivariate data analyses and models. Both unsupervised and supervised analyses were conducted using the Ropls package in R software (Thévenot et al., 2015). Models were built on principal component analysis (PCA), partial least squares-discriminant analysis (PLS-DA), and orthogonal partial least squares-discriminant analysis (OPLS-DA). All the models evaluated were tested for over fitting with methods of permutation tests. The descriptive performance of the models was determined by R2X (cumulative) (perfect model: R2X (cum) = 1) and R2Y (cumulative) (perfect model: R2Y (cum) = 1) values, while their prediction performance was measured by Q2 (cumulative) (perfect model: Q2 (cum) = 1) and a permutation test.

2.4. Identification and selection of significantly differential metabolites

Metabolites were putatively identified based on a comparison of their retention time (RT), as well as m/z and MS/MS spectra that matched with the Human Metabolites Database (HMDB) (http://www.hmdb.ca), MassBank (http://www.massbank.jp/), LipidMaps (http://www.lipidmaps.org), mzcloud (https://www.mzcloud.org), Kyoto Encyclopedia of Genes and Genomes (KEGG) (http://www.genome.jp/kegg) and the metabolite database of Panomix Biomedical Tech Co., Ltd. (Shuzhou, China). The p-value, variable importance in projection (VIP) produced by OPLS-DA, and fold change (FC) were applied to determine the variable contribution for the abundance of metabolites in the comparison of DFB vs CK (DC), DFB vs HFB (DH) and HFB vs CK (HC). Finally, metabolites with $P < 0.05$ and VIP>1 were considered to be statistically significant, and those metabolites that have been reported from microorganisms with $|\log_2 FC|>4$ (FC > 16 or FC < 0.0625) were selected as candidates for further functional analyses. Correlation analysis of these candidates was conducted by calculating the Pearson's correlation coefficient of each metabolite.

2.5. Metabolic pathway and BGC analyses

Metabolites only altered in the diseased part ($|\log_2 FC|>4$ in both DC and DH and $|\log_2 FC|<2$ in HC) were considered to be significant metabolites during the infection process, while those only in the healthy part ($|\log_2 FC|>4$ in DC and HC and $|\log_2 FC|<2$ in DH) were metabolites involved in the host response. Chemical structures and reported biological activities of metabolites were obtained from PubChem (https://pubchem.ncbi.nlm.nih.gov/) and previous publications. Metabolic pathways associated with those functional metabolites were obtained from the KEGG database and previous publications. Information on reference proteins involved in the investigated pathways was obtained from the KEGG and UniProt (https://www.uniprot.org/) databases. Protein sequences obtained from the genomic data of *Ca. arbuscula* NRRL 3705 (ASM982864v1) and *C. militaris* (CmilitarisCM01_v01) were further matched using the tBLASTn in NCBI, as the genomic data of *Ca. cordycipiticola* (PRJNA766243) in GenBank is not assembled (Cheng et al., 2020; Zheng et al., 2011).

To identify the responsible BGCs, the pathogen genomes were first

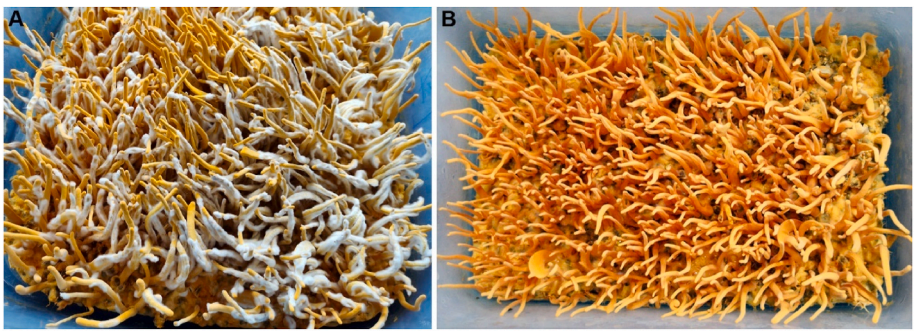

Fig. 1. Diseased fruiting bodies (A) and healthy fruiting bodies (B) of *Cordyceps militaris* used in this study.

annotated using the fungal version of antiSMASH version 7.0 (https://antismash.secondarymetabolites.org/) and the proper reference. Homology analysis between two modules BGC (BGC0000011 and BGC0000152) from *Aspergillus* spp., and the detected BGC in the *Ca. arbuscula* genome was then conducted with clinker via the CompArative GEne Cluster Analysis Toolbox (CAGECAT) (van den Belt et al., 2023).

2.6. Verification of significant metabolites

Candidate metabolites that were suspected to be the virulence factors were further analyzed separately on an HPCL system (1260 Infinity II LC System Agilent, USA) using a C18 column (ZORBAX SB 250 mm × 4.6 mm, 5 μm, Agilent, USA) with a sample injection volume of 10 μL. All samples were filtered through a microporous membrane (0.45 μm) before detection. The standards of aflatoxin B1 (AFB1) (1 mg), and sterigmatocystin (ST) (1 mg), were purchased from Guizhou Senzhiyuan Agricultural Technology Co., Ltd. and dissolved in 50 % methanol and 90 % acetonitrile, respectively.

AFB1 detection: The sample for detecting AFB1 was extracted by mixing 10 g of dried *C. militaris* powder, 3 g of sodium chloride, and 75 mL of 70 % methanol into a 250 mL reaction tube, which was then stirred at 12,000 rpm for 2 min and centrifuge at 2500 rpm for 5 min. The mobile phase for detecting AFB1 consisted of 4:1 (v/v) 50 % methanol and acetonitrile with a constant flow rate of 1 mL/min. The temperature of the column was kept at 30 °C and UV–Vis data was recorded with a diode array detector (DAD) at 365 nm and 450 nm.

ST Detection: The sample for detecting ST was first extracted by mixing 5 g of dried *C. militaris* powder with 25 mL acetonitrile into a 50 mL centrifuge tube, which was then vortexed for 1 min and sonicated for 7 min. Afterward, 1 g anhydrous $MgSO_4$ and 1 g NaCl were added and mixed, followed by centrifuging at 4500 rpm for 5 min. Finally, the supernatant was mixed with 50 mg primary secondary amine (PSA) and centrifuged at 4500 rpm for 5 min. The mobile phase for detecting ST consisted of a combination of 0.1 % formic acid and acetonitrile with a constant flow rate of 1 mL/min. The gradient elution process began with 50 % acetonitrile for 10 min and gradually increased to 50–100 % acetonitrile for 20 min. The temperature of the column was kept at 40 °C and UV–Vis data was recorded with a DAD at 238 nm.

3. Results

3.1. Data processing and identification of differential metabolites

The LC-MS/MS analysis detected 11,054 positive ion features and 12,448 negative ion features after normalization. Results from PCA, PLS-DA, and OPLS-DA all revealed an evident separation of the three groups in either positive or negative ionization mode, suggesting a significant difference in the metabolic profiles of the tested groups (Fig. 2). Afterwards, 513 differential metabolites were putatively identified among the three groups through MS/MS analysis. (Fig. 3), with the distribution of significantly differential metabolites ($P < 0.05$ and VIP>1) among the three groups shown in Fig. 4. After screened by the variable contribution, 50 candidate metabolites were finally selected for further analyses (Table 1). Most of the candidate metabolites are positively correlated to others, with the exception of some nucleotides and amino acids (Fig. 5).

3.2. Key metabolites and metabolic pathways related to the infection process

There are 17 significant metabolites and 24 pathways found in the infection process of the pathogen (Fig. 6). An AFB1-like compound (*m/z* = 311.0597, RT = 694.2 s) is the most notably elevated first metabolite during the infection, which is the only mycotoxin accumulated in the diseased part. AFB1 is the most hepatotoxic and carcinogenic of the AFs. Its cytotoxicity is implicated in the pathways of excess reactive oxygen species (ROS) production, DNA damage, oxidative stress, lipid peroxidation, apoptosis, mitochondrial dysfunction, autophagy, necrosis, and inflammatory response (Dai et al., 2022; Wu et al., 2024; Geng et al.,

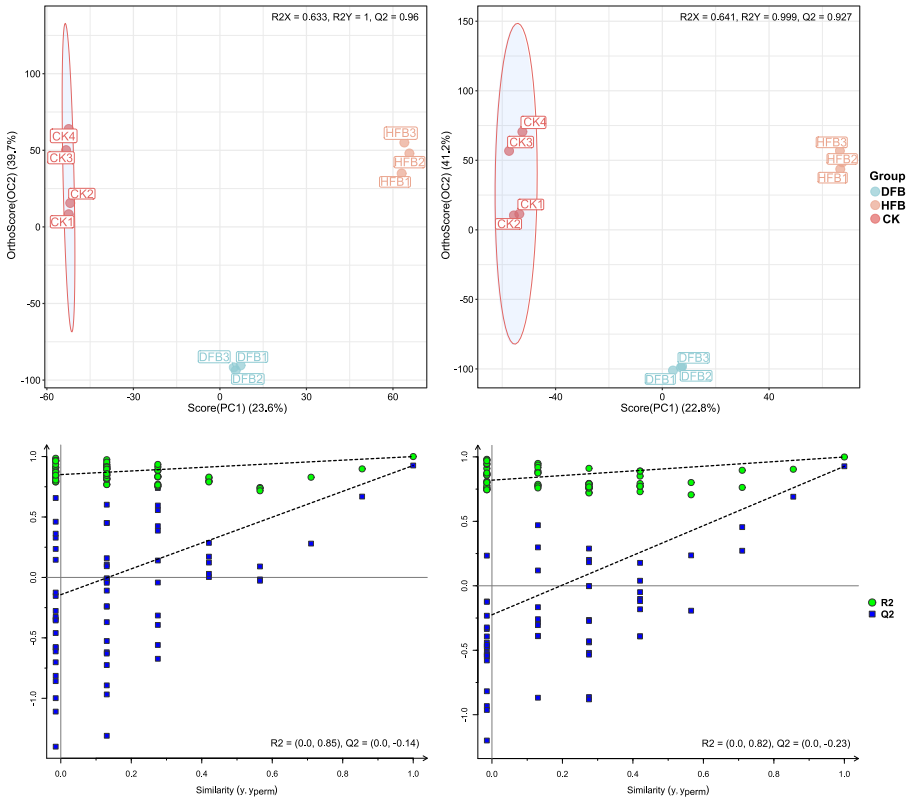

Fig. 2. OPLS-DA score plot and permutation test for positive ion (A, C) and negative ion (B, D) of DFB, HFB, and CK group.

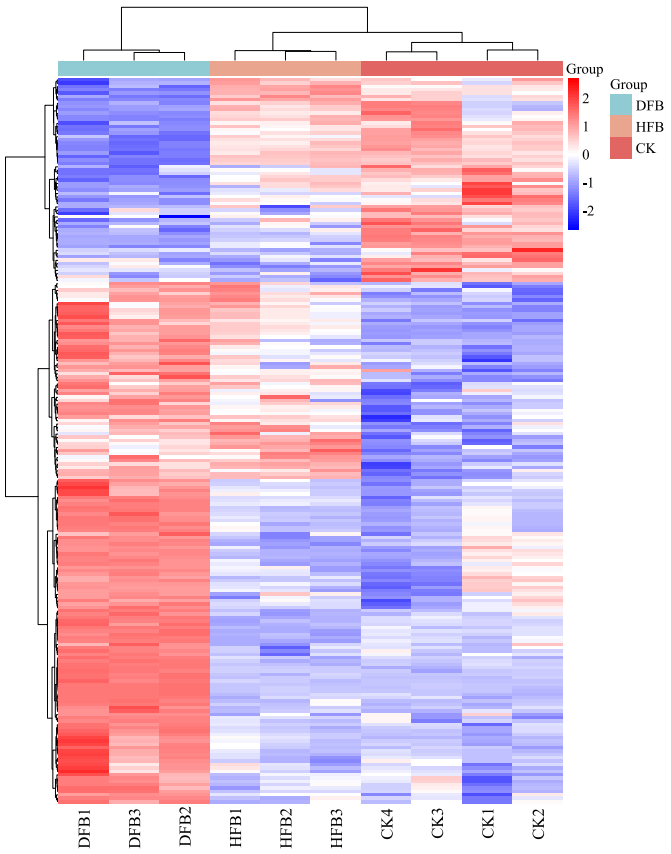

Fig. 3. Heatmap following a hierarchical clustering of differential metabolites among CK (1–4 replicates), DFB (1–3 replicates), and HFB (1–3 replicates), which displays the abundance of 513 metabolites putatively identified by LC-MS/MS analysis. Scaled abundance is color-coded from red (high abundance) to dark blue (low abundance). The R package heatmap generated the dendrogram. (For interpretation of the references to color in this figure legend, the reader is referred to the Web version of this article.)

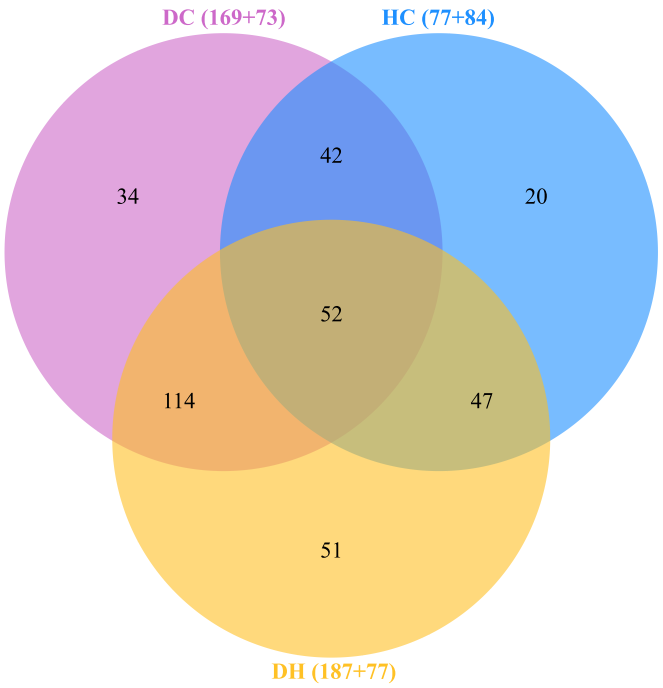

Fig. 4. Venn diagram showing the number and relationship of significantly differential metabolites ($P < 0.05$, VIP>1) among DC (DFB vs. CK), HC (HFB vs. CK), and DH (DFB vs. HFB) groups. Numbers in brackets indicate the number of up and down-regulated metabolites, respectively.

2024).

The second metabolite with significantly increased abundance is a 3-methyl-2-oxovaleric acid-like compound (m/z = 131.0704, RT = 558.9 s), which is produced from isoleucine by cytosolic branched chain aminotransferase 1 and plays a critical role in neurological damage (Wang et al., 2019). It can also be a specific inhibitor for O_2^-/H_2O_2 production by KGDHC, which decreases ROS during α-ketoglutarate and pyruvate oxidation (Slade et al., 2017).

The most significantly decreased metabolite in the diseased part was a compound of the type D-myo-inositol 3,4,5,6-tetrakisphosphate (Ins (3,4,5,6)P4) (m/z = 480.9091, RT = 63.4 s), multifunctional signaling molecule produced by 1D-myo-inositol 1,3,4,5,6-pentakisphosphate (Ins(1,3,4,5,6)P5) in the metabolism of myo-inositol phosphate, the intermediate products of which are involved in various cellular metabolic pools as well as in signal transduction (Chatree et al., 2020; Eckmann et al., 1997; Sahu et al., 2024; Sauer and Cooke, 2010). Ins(1,3,4,5,6)P5 is also the precursor of phytic acid, an antifungal agent, as well as the end product of myo-inositol phosphate metabolism pathway, which has the impact on regulating glycerophospholipid metabolism through several mechanisms such as a signaling molecule, modulation of phospholipase activity and activation of certain kinases (Chatree et al., 2020; Ghoshal et al., 2016; Li et al., 2023; Sahu et al., 2024). Reduction of Ins (3,4,5,6)P4 may indicate a metabolic disorder or death of cells in the diseased part after infection.

Both pathways of AFB1 and polyamine biosynthesis are indicated to be functional during the infection (Fig. 7). Activation of AFB1 biosynthetic pathway is suspected to be relevant to the initial infection process, whereas polyamines such as putrescine, spermidine, and spermine are small, ubiquitous organic polycations (having a positive charge on each nitrogen atom) found in archaeal, eubacterial and eukaryotic cells, which plays an important role in cell growth, cell proliferation, differentiation, nucleic acid synthesis.

3.3. Verification of key metabolites during the infection

To further confirm the accumulated mycotoxin in the diseased part, the complete biosynthetic pathway of AFB1 was analyzed based on the module of *Aspergillus flavus* NRRL3357 in KEGG (accessed on May 2023), and the homology analysis between module ST BGCs and the detected BGC in the *Ca. arbuscula* genome was conducted. The pathogen has homologs in its genome with high similarities to enzymes involved in the AFB1 synthesis pathway, whereas those in the host genome were poorly matched (Fig. 8). This indicates that the pathogen has an almost complete set of ABF1 synthetic genes, except for the last two steps that start from ST. The synteny analysis also showed high degree of conservation for the core biosynthetic genes involved in ST biosynthesis, which implies that the product from contig31 in the *Ca. arbuscula* genome belongs to the ST mycotoxin class (Fig. 9). ST is the precursor for AFB1 biosynthesis, which also shares a similar cytotoxicity with AFB1, such as increasing ROS level and inducing DNA damage (Zingales et al., 2020). Therefore, a ST-like metabolite is indicated as a suspected virulent factor, produced by *Ca. cordycipiticola*, during the infection process, as the genome of *C. militaris* does not contain genes for known mycotoxins (Zheng et al., 2011).

To further confirm the absence of ST or AFB1, we compared the LC-MS profiles from the extracts obtained from DFB with authentic standards from these mycotoxins. However, these two molecules were not found within the analyzed extracts (Fig. S1), which agrees with the hypothesis that *Ca. arbuscula* might produce yet unknown but related toxins.

Table 1
Information of significant metabolites during the infection process of *Ca. cordycipiticola* and host response of *C. militaris*.

KEGGID	Compounds	Comparison	log2FC	-log10P	VIP	Ion mode
C12136	(−)-Epigallocatechin	HC	4.91	2.81	1.51	pos
C08491	(−)-Jasmonic acid	HC	−7.03	4.74	1.59	neg
C08491	(−)-Jasmonic acid	DH	5.55	5.26	1.22	neg
C20279	(2R,3R)-3-Methylglutamyl-5-semialdehyde-N6-lysine	DH	4.23	1.59	1.17	pos
C05161	(2R,5S)-2,5-Diaminohexanoate	DC	4.94	4.71	1.42	pos
C09947	(R)-Kawain	DC	5.35	2.12	1.32	pos
C09947	(R)-Kawain	DH	5.28	5.01	1.24	pos
C02774	10-Hydroxydecanoic acid	DC	−4.03	1.9	1.28	neg
C01226	12-OPDA	HC	−6.46	2.6	1.48	neg
C01226	12-OPDA	DH	5.1	1.79	1.18	neg
C13857	1-Arachidonoylglycerol	HC	−9.99	1.8	1.36	pos
C13857	1-Arachidonoylglycerol	DH	7.79	2.53	1.18	pos
C05853	2-Phenylethanol	DC	4.83	2.45	1.37	pos
C05576	3,4-Dihydroxyphenylglycol	DH	4.06	5.62	1.24	pos
C03465	3-Methyl-2-oxovaleric acid	DC	8.68	8.42	1.43	pos
C03465	3-Methyl-2-oxovaleric acid	DH	8.86	6.58	1.24	pos
C01179	4-Hydroxyphenylpyruvic acid	DH	4.72	2.44	1.21	neg
C20773	6-Amino-6-deoxyfutalosine	HC	5.06	2.16	1.48	neg
C14825	9,10-Epoxyoctadecenoic acid	DH	−4.04	3.04	1.19	neg
C00008	Adenosine diphosphate	HC	−4.8	2.71	1.49	neg
C00008	Adenosine diphosphate	DH	4.52	3.46	1.20	neg
C06800	Aflatoxin B1	DC	10.13	3.01	1.39	neg
C06800	Aflatoxin B1	DH	9.19	1.69	1.17	neg
C00179	Agmatine	DC	6.02	5.52	1.43	pos
C00179	Agmatine	DH	7.34	4.3	1.23	pos
C06427	α-Linolenic acid	DC	−4.95	7.52	1.43	neg
C06427	α-Linolenic acid	DH	−4.82	4.56	1.22	neg
C06425	Arachidic acid	DH	−4.16	2.82	1.20	pos
C09815	Benzamide	HC	−6.05	2.88	1.51	neg
C09815	Benzamide	DH	7.04	1.68	1.17	neg
C00719	Betaine	DC	4.97	2.68	1.43	pos
C00719	Betaine	DH	4.79	3.94	1.23	pos
C06327	Chelirubine-like	DC	4.54	3.2	1.38	pos
C06327	Chelirubine-like	HC	4.71	2.76	1.55	pos
C11379	Cinchonidine	DC	6.7	6.55	1.43	pos
C11379	Cinchonidine	DH	6.82	4.25	1.23	pos
C00055	Cytidine monophosphate	DH	−5.52	4.69	1.23	pos
C00559	Deoxyadenosine	HC	−6.18	5.94	1.60	pos
C05512	Deoxyinosine	HC	−5.48	2.15	1.42	pos
C05512	Deoxyinosine	DH	5.87	4.75	1.23	pos
C00526	Deoxyuridine	DC	−5.51	2.08	1.27	pos
C00526	Deoxyuridine	HC	−4.52	1.63	1.31	pos
C04520	D-Myo-inositol 3,4,5,6-tetrakisphosphate	DC	−8.78	4.7	1.41	neg
C04520	D-Myo-inositol 3,4,5,6-tetrakisphosphate	DH	−9.25	4.47	1.22	neg
C00379	D-Xylitol	DC	6.03	2.75	1.33	neg
C09263	Esculetin	DC	4.03	2.51	1.33	pos
C18319	Ethylmethylacetic acid	DC	7.33	6.57	1.43	pos
C18319	Ethylmethylacetic acid	DH	7.95	4.16	1.23	pos
C00262	Hypoxanthine	DC	6.62	3.57	1.42	pos
C00262	Hypoxanthine	DH	6.36	6.79	1.24	pos
C02993	Kyotorphin	DC	4.75	3.76	1.41	pos
C02993	Kyotorphin	DH	4.03	2.86	1.20	pos
C05519	L-Allothreonine	HC	5.95	7.53	1.60	pos
C05519	L-Allothreonine	DH	−5.51	7.98	1.24	pos
C00073	L-Methionine	HC	4.36	2.14	1.47	pos
C07570	Mirtazapine	DH	4.66	1.98	1.21	pos
C00455	Nicotinamide ribotide	DC	−4.15	1.42	1.14	pos
C05954	Prostaglandin B2	DC	−4.33	3.01	1.37	pos
C00314	Pyridoxine	HC	−4.62	2.98	1.57	pos
C00396	Pyrimidine	DC	−4.82	2.37	1.31	pos
C06526	Quinine	DH	4.25	2.37	1.17	pos
C00474	Ribitol	DH	4.17	1.92	1.11	neg
C03431	*S*-Inosyl-L-homocysteine	DC	5.83	3.97	1.42	neg
C03431	*S*-Inosyl-L-homocysteine	DH	4.82	2.1	1.20	neg
C03172	*S*-Methyl-L-methionine	DC	4.83	2.72	1.33	pos
C03172	*S*-Methyl-L-methionine	HC	4.45	2.34	1.45	pos
C00089	Sucrose	DC	−4.3	3.62	1.39	neg
C01494	trans-Ferulic acid	DH	4.5	6.42	1.22	neg
C01456	Tropate	HC	4.44	3.53	1.55	pos
C01456	Tropate	DH	−4.46	4.11	1.23	pos
C00977	Tryptophanamide	DC	5.47	7.01	1.42	neg
C00977	Tryptophanamide	DH	5.3	6.11	1.22	neg
C06044	Tyrosol	DC	4.86	5.74	1.43	pos
C06044	Tyrosol	DH	6.47	4.9	1.24	pos
C00043	Uridine diphosphate-N-acetylglucosamine	DC	−4.15	3.69	1.39	neg

pos: positive ion mode; neg: negative ion mode.

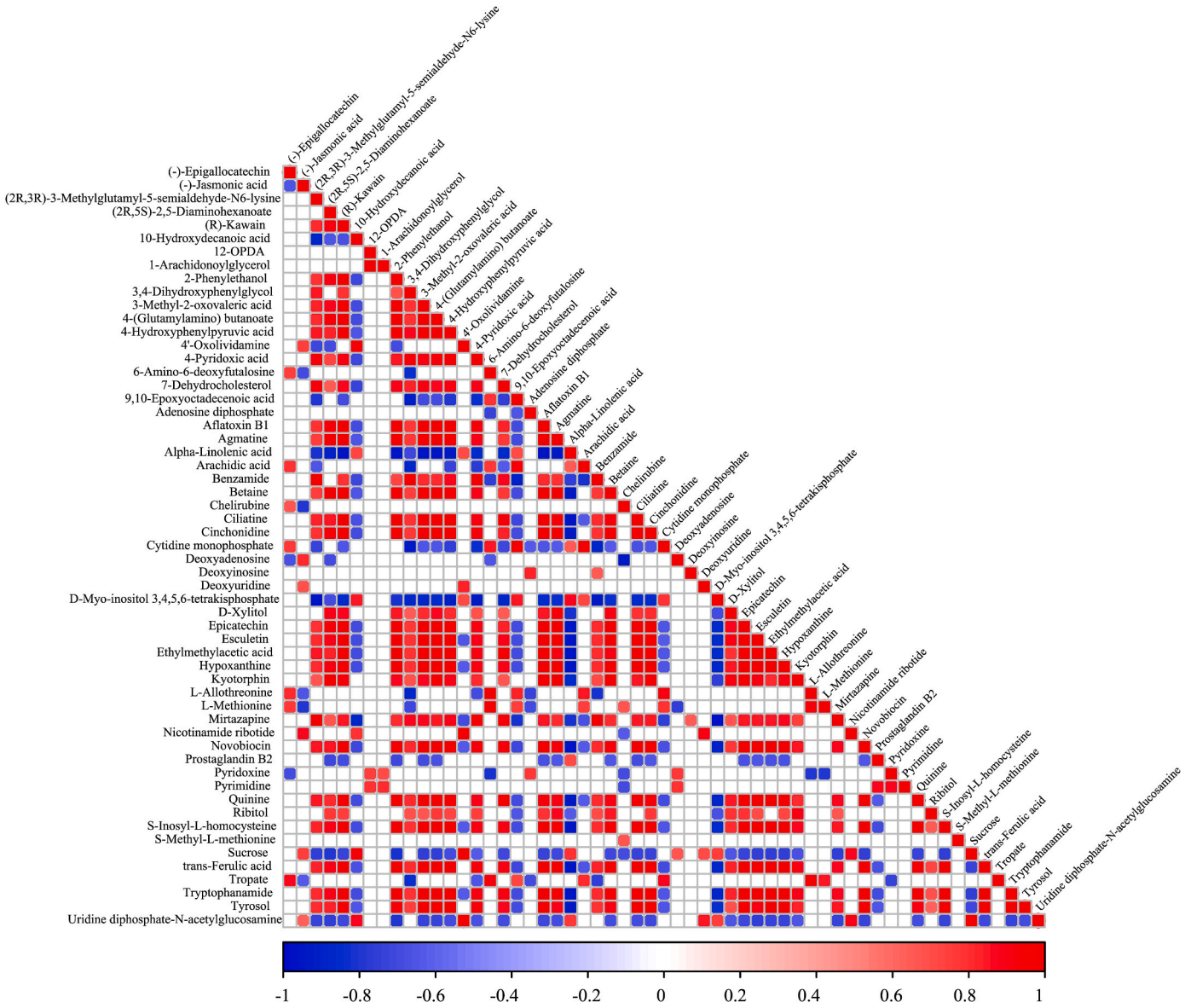

Fig. 5. The correlation heatmap following an average linkage hierarchical clustering of candidate metabolites generated by R package correplot. The Pearson correlation coefficient and P were calculated using cor and cor.test functions respectively. Positive and negative correlation ($P < 0.05$) is represented by red and blue colors, respectively. (For interpretation of the references to color in this figure legend, the reader is referred to the Web version of this article.)

3.4. *Metabolites involved in the host response to the infection*

There are three significant metabolites, and five pathways found in the host response to the infection (Fig. 10). The most significantly decreased metabolite is a 2′-deoxyuridine (dU)-like compound (m/z = 228.1956, RT = 778.2 s), a significant intermediate in nucleotide metabolism, especially pyrimidine metabolism, which is relevant to enzymatic regulation and DNA repairing, as well as acting as an infection-promoting factor during interactions between plants and fungal pathogens (Ando et al., 2010; Armenta-Medina et al., 2014; Cui et al., 2019). It forms a dynamic equilibrium with uracil, uridine, and uridine triphosphate (UTP), and finally affects the abundance of L-glutamine. Since the genomes of parasitic pathogens lack complete pyrimidine metabolic equipment (Garavito et al., 2015), deoxyuridine depletion may result from a lack of metabolic resources by the pathogen, as well as a means by which the host resists infection.

A *S*-methyl-L-methionine (SMM)-like compound (m/z = 165.0758, RT = 137 s) is the most significantly increased metabolite in the host response. SMM, sometimes referred to as vitamin U, is an extensive regulator in plant physiological processes, especially being an important donor of methyl and sulfur and enhancing plant resistance to abiotic and biotic stress factors (Fodorpataki et al., 2019; Ludmerszki et al., 2015; Saint-Macary et al., 2015; Szegő et al., 2007). SMM can also be catalyzed by homocysteine *S*-methyltransferase (HMT) to form L-methionine (Met), an essential amino acid with a critical role in the metabolism and health of many species, but this reaction occurs exclusively in host cells (Fig. 11).

The second metabolite with significantly increased abundance is a chelirubine-like compound (m/z = 362.0838, RT = 295.2 s). Chelirubine is a parent hydride of sanguinarine (Croaker et al., 2022; Jiao et al., 2024) that can effectively inhibit the growth of fungal pathogens by destroying the integrity of cell membranes and obstructing the

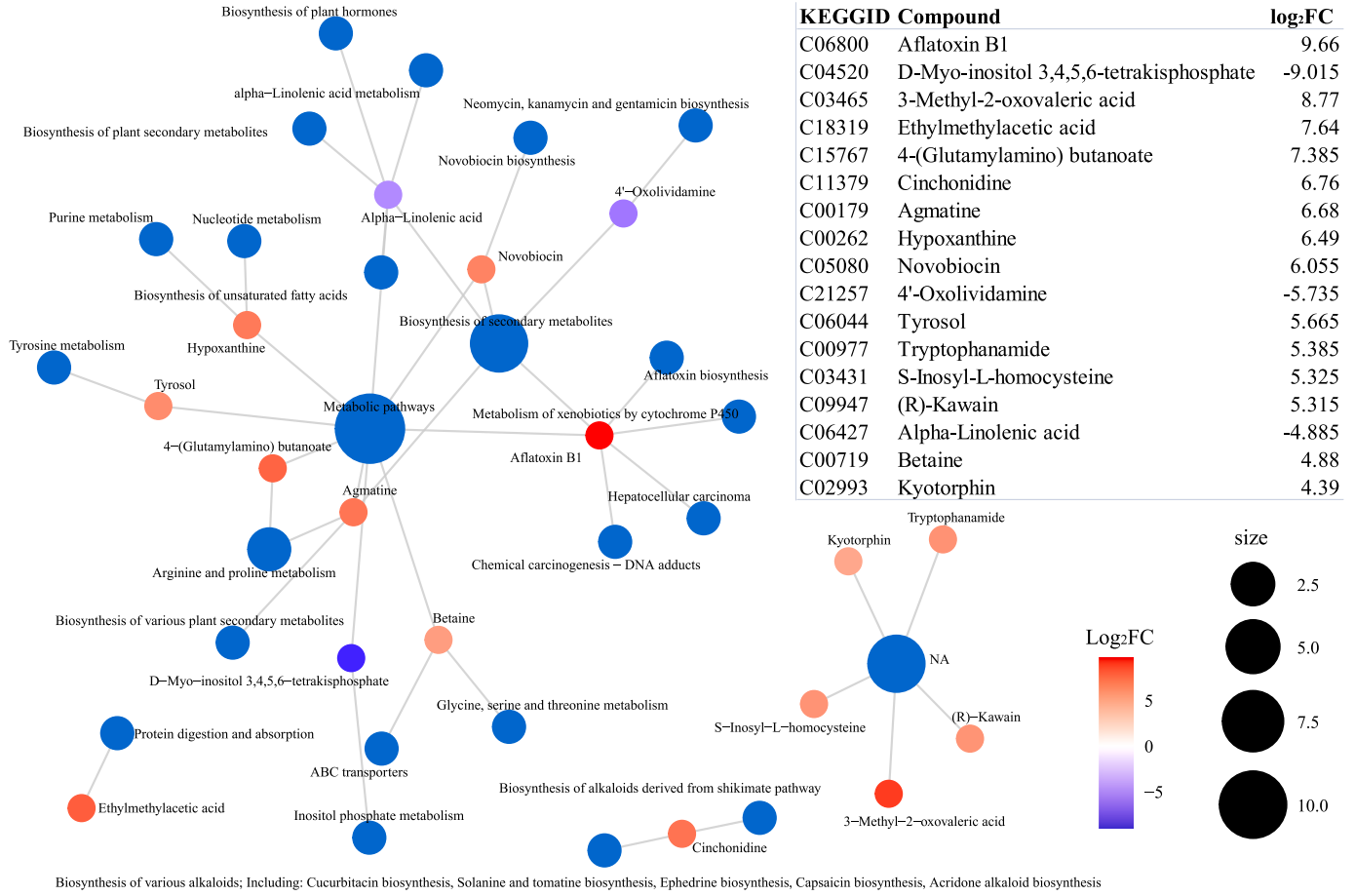

KEGGID	Compound	log_2FC
C06800	Aflatoxin B1	9.66
C04520	D-Myo-inositol 3,4,5,6-tetrakisphosphate	-9.015
C03465	3-Methyl-2-oxovaleric acid	8.77
C18319	Ethylmethylacetic acid	7.64
C15767	4-(Glutamylamino) butanoate	7.385
C11379	Cinchonidine	6.76
C00179	Agmatine	6.68
C00262	Hypoxanthine	6.49
C05080	Novobiocin	6.055
C21257	4'-Oxolividamine	-5.735
C06044	Tyrosol	5.665
C00977	Tryptophanamide	5.385
C03431	S-Inosyl-L-homocysteine	5.325
C09947	(R)-Kawain	5.315
C06427	Alpha-Linolenic acid	-4.885
C00719	Betaine	4.88
C02993	Kyotorphin	4.39

Fig. 6. The relevant pathway-compound network during the infection process. Compounds in the list are arranged in order of the mean $|log_2FC|$ values from two comparisons.

function of mitochondria and the nucleus (Hu et al., 2022; Zhao et al., 2019), as well as having anti-inflammatory activities. The production of these benzophenanthridine alkaloids may be generated by the host to resist fungal pathogens. So far to the best of our knowledge, benzophenanthridine alkaloids are only found in plants and future studies are required to verify the existence of an alternate pathway in fungi.

4. Discussion

White mildew disease caused by *Ca. cordycipiticola* has become a severe problem leading to serious economic losses for the *C. militaris* industry (Liu et al., 2021). Most pathogenic fungi have undergone different expansion processes related to gene families facilitating host infection, including proteases, secreted proteins, cell wall degrading enzymes, antimicrobial detoxification enzymes, and secondary metabolites (Aguileta et al., 2009). For example, *Penicillium marneffei* is rich in BGCs and thioester-mediated non-ribosomal protein synthesis (Yuen et al., 2003). In contrast, *Ustilago maydis*, a basidiomycete that parasitizes maize, possesses secreted protein effectors favoring the invasion of living tissue while minimizing host damages (Kämper et al., 2006). Both genomes of *Ca. arbuscula* and *Ca. cordycipiticola* contains the dimethylcoprogen BGC, which is responsible for the biosynthesis of coprogens and required for inhibiting pathogenic fungi (Cheng et al., 2020; Liu et al., 2021; Severn-Ellis et al., 2022). These compounds are siderophores (Chen et al., 2013; Severn-Ellis et al., 2022) mainly produced under iron-limited conditions; so, it was not surprising to us that we could not detect them in the infected tissues. In addition to the previously mentioned antifungals, there are other compounds with significantly increased abundance, including intermediates and fatty acids. For example, ethylmethylacetic acid, which is an intermediate metabolite found in bacteria, fruits, and humans, is also a volatile compound produced by *Bacillus* spp. that exhibits antifungal activity (Martins et al., 2019; Xu et al., 2021). In addition, a significant increase of 4-(glutamylamino) butanoate and *S*-inosyl-L-homocysteine (SIH), compounds involved in the pathway of only prokaryotes; especially SIH an uncommon metabolite found in the *S*-adenosyl-L-methionine (SAM) recycling of *Methanocaldococcus jannaschii* (Miller et al., 2015), indicates the existence of co-inhabiting archaea in the diseased part when cultivation.

4.1. Key virulence factors during the infection process

In addition to common cell wall-degrading enzymes, various infection strategies are used by different mycoparasites (Liu and Dong, 2023). Hypocreales species, to which *Ca. cordycipiticola* belongs, are a source of potent food and grain-contaminating mycotoxins that are widespread in cereal crops, leading to yield losses and severe diseases (Rossman, 1996; Shank et al., 2011; Urbaniak et al., 2019). Species within the Hypocreales can produce AF-like toxins such as AFB1 and ST (Bradshaw et al., 2006; Cheng et al., 2020). Additionally, AF and ST have also been isolated from the genus *Aschersonia* (Clavicipitaceae, Hypocreales) (Zhang et al., 2020). These studies demonstrate that species of Hypocreales have the ability to produce AF-like toxins and other mycotoxins.

Our results of the metabolomics detection and the analysis of relevant pathways together with the comparison of BGCs indicated a very strong possibility that an ST-like metabolite, synthesized by the pathogen, acts as the virulence factor during the infection. The present data would suggest that the *Ca. arbuscula* BGC can not produce AFB1, and the relatively low homology of some enzymes might indicate that the fungus

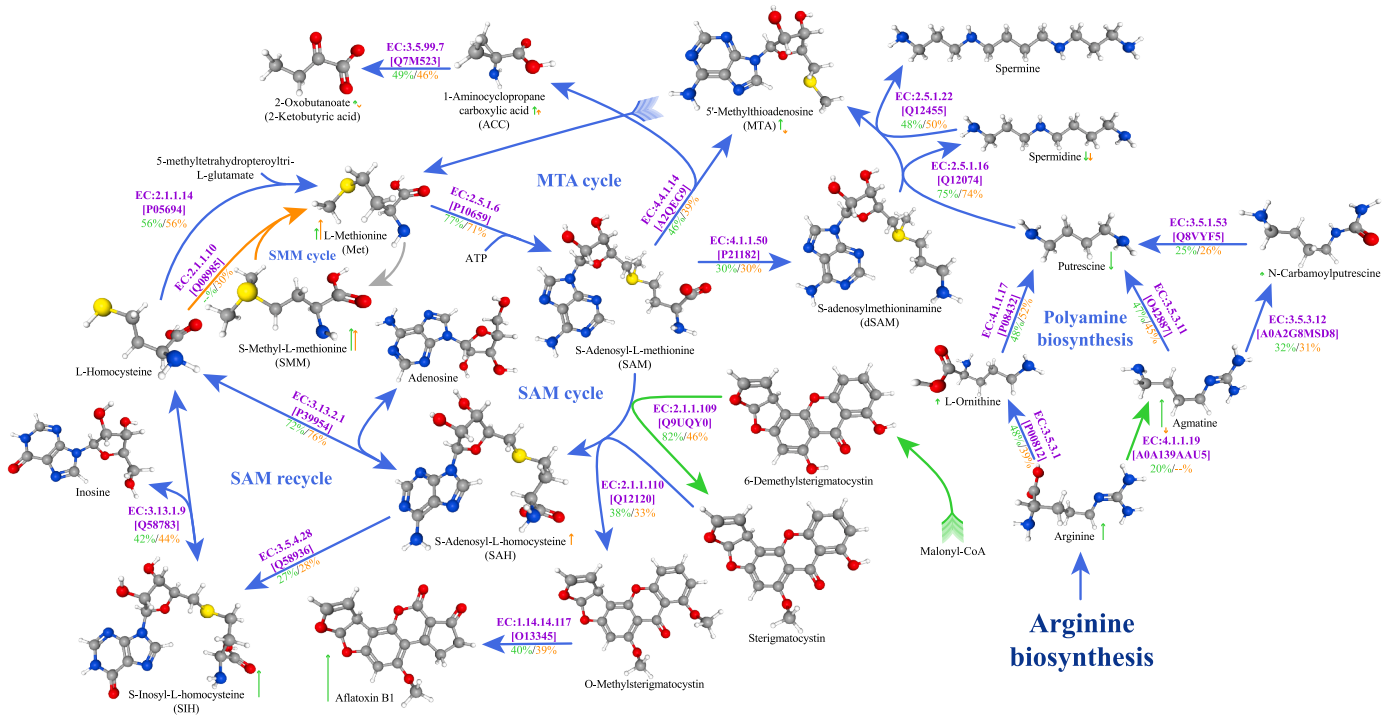

Fig. 7. Relevant pathways during the infection process. Proteins catalyzing each reaction are displayed in purple between the AFB1 and polyamine compounds, with corresponding enzyme codes or names shown above and the reference UniProtKB entries in brackets. The similarity of homologs in the pathogen and host genome to protein sequences of reference enzymes is displayed in lime green and dark orange color below the information on enzymes. Arrows (tails indicate multiple reactions) between each two compounds indicate the direction of reactions, with their occurrence indicated in royal blue (both pathogen and host), lime green (only pathogen), dark orange (only host) and grey (neither pathogen and host) color. Arrows next to the compound indicate the variation of abundance in DC (lime green) and HC (dark orange). (For interpretation of the references to color in this figure legend, the reader is referred to the Web version of this article.)

could produce something related but still not the same molecules.

Mycotoxins, such as ochratoxin and Afs (NRCC, 1985; Kelman et al., 2024), have been shown to act as pathogenicity factors and virulence factors in some fungal infections of insects and plants (Hof and Kupfahl, 2009), even with low concentrations (Omar et al., 2020). Infection of *Ca. cordycipiticola* begins with the invasion of pathogenic hyphae between the interstices of the host mycelium, producing micropores at the interface and causing deformation of the host cells (Liu et al., 2021) This targeted infection strategy allows infection to occur only under a deficient concentration of virulence substances. On the other hand, these toxins are not stable under certain physical, chemical, or biological conditions (Guo et al., 2021), which might lead to their degradation or transformation into other compounds (Tahir et al., 2018), as well as they are not being detected (Zhang and Banerjee, 2020). Our results above indicate that an ST-type metabolite is one of the virulence factors of downy mildew disease in *C. militaris*, but further investigation is needed, especially to identify it.

4.2. Metabolic pathways

In the case of *Ca. cordycipiticola* infecting *C. militaris*, ST-like and sanguinarine-like biosynthesis are indicated to be the key pathways in the process of pathogen infection and host response, respectively, with SAM being a key intermediate compound (Figs. 7 and 11). SAM is a universal methyl donor involved in numerous biological processes, including DNA methylation, protein methylation, and neurotransmitter synthesis, as well as a crucial molecule in various biological processes in host–pathogen interactions (Kawalleck et al., 1992). The SAM-dependent decarboxylation reaction has been shown to be a necessary step in the catalytic synthesis of blasticidin S (BLS), a peptidyl nucleoside antibiotic produced by *Streptomyces griseochromogenes* and widely used in protection against rice blast diseases (Feng et al., 2013; Liu et al., 2017; Gannett et al., 2024). SAM is also an essential methyl donor in the biosynthesis of phytohormone methyl jasmonate (MeJA), which can inhibit the hyphal growth of *Sporisorium scitamineum* (causing sugarcane smut) and *U. maydis* (causing maize smut) under *in vitro* culture conditions (Cui et al., 2023). In Hypocreales, SAM also plays an important role in the biosynthesis of mycotoxins and other bioactive secondary metabolites (Domínguez-Santos et al., 2022; von Döhren, 2004).

Enzymes involved in the SAM cycle play essential roles in methylation metabolism, fungal development, full virulence, multiple stress responses, lipid metabolism, and fungicide sensitivity (Ogihara et al., 2020). SAM is synthesized from Met and ATP by the *S*-adenosylmethionine synthetase enzyme (EC:2.5.1.6), and its sulfonium functional group is the center of its peculiar reactivity. Depending on the enzyme, SAM can be converted into *S*-adenosyl-L-homocysteine (SAH), *S*-adenosylmethioninamine (dSAM) and 5′-methylthioadenosine (MTA) catalyzed by SAM-dependent methylases (EC:2.1.1), adenosylmethionine decarboxylase (EC:4.1.1.50) and 1-aminocyclopropane-1-carboxylate synthase (EC:4.4.1.14). SAM-derived products can finally be recycled to regenerate SAM through the SAM or MTA cycles (Fig. 7 and 12). SAM can also react with Met under the catalyzation of Met *S*-methyltransferase (MMT), generating SMM and SAH, and the mutual conversion of Met and SMM forms the SMM cycle, which operates throughout the plant and consumes half of the SAM produced in *Arabidopsis* leaves (Kocsis et al., 2003; Peng et al., 2022). However, the protein sequence of MMT did not match the genome of the pathogen or host (Fig. 11). Another pathway related to SAM, connected with dSAM, is polyamine biosynthesis, in which the abundance of arginine, agmatine, L-ornithine, putrescine and spermidine were significantly altered during the infection process (Fig. 7). In our study, the low similarities of some enzymes catalyzing different reactions in significant pathways are due to the distance between modular pathway taxa.

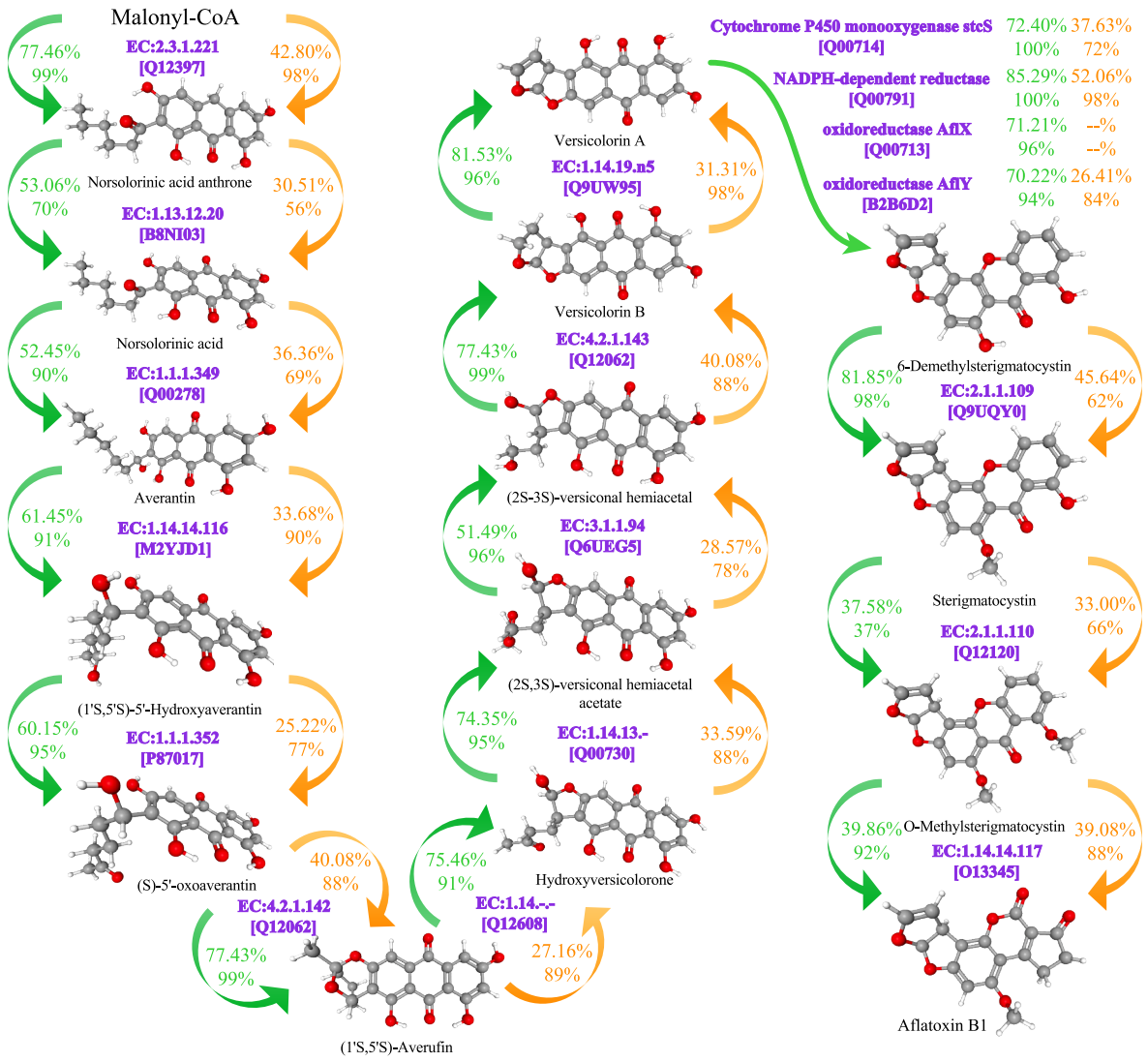

Fig. 8. AFB1 biosynthetic pathway of *Aspergillus*. Proteins catalyzing each reaction are displayed in purple between the two compounds, with corresponding enzyme codes or names shown above and reference UniProtKB entries in the bracket. Arrows indicate the direction of reactions, and the percentages indicate the similarity and coverage of homologs in the studied genomes to protein sequences of reference enzymes. The lime green color represents the pathogen, and the dark orange color represents the host. (For interpretation of the references to color in this figure legend, the reader is referred to the Web version of this article.)

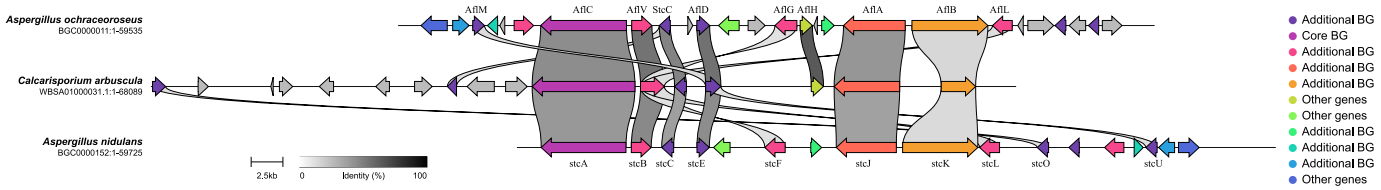

Fig. 9. Synteny analysis between the contig31 of *Ca. arbuscula* genome and related ST BGC identified from *Aspergillus* spp.

4.3. Food security

ST shares structural and biological similarities with AFB1 (Szabó et al., 2024), one of the deadliest mycotoxins capable of inducing hepatotoxicity, nephrotoxicity, neurotoxicity, immunotoxicity, and reproductive toxicity, which can lead to various acute or chronic diseases, such as cancer, hepatitis, mutation abnormalities, and reproductive disorders (Alonso-Jauregui et al., 2023; Dai et al., 2022; Díaz Nieto et al., 2018; Rushing and Selim, 2019; Zingales et al., 2020, 2024). Other compounds accumulated after infection have also been reported as toxic to humans, including 3-methyl-2-oxovaleric acid (Wang et al., 2019) and sanguinarine (Singh and Sharma, 2018; Yang et al., 2021). Therefore, the fruiting bodies of *C. militaris* infected by *Ca. cordycipiticola* are inedible.

5. Conclusions

This study examines the complex scenario of key metabolic biosynthesis in the pathogenic mechanisms of *Ca. cordycipiticola* in relation to *C. militaris*. An ST-like metabolite is identified as one of the virulence factors of white mildew disease in *C. militaris*. However, it is the SAM cycle that emerges as a key player, playing a central role in both

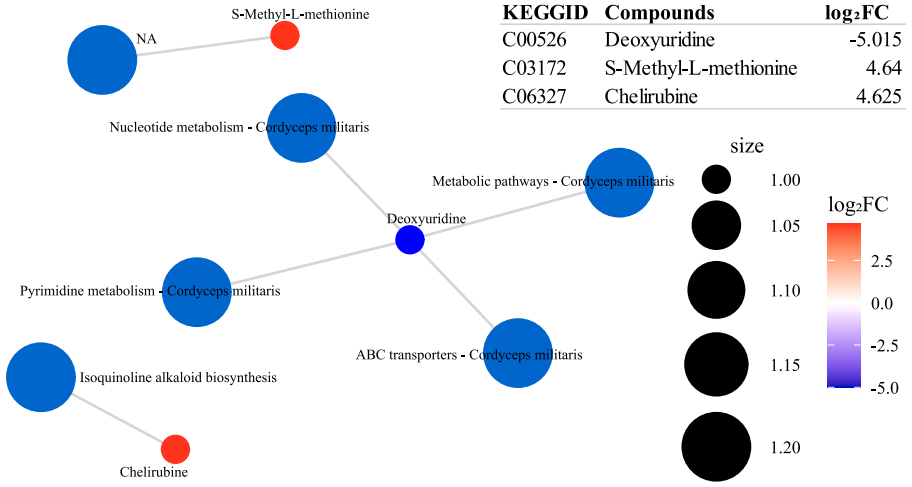

KEGGID	Compounds	log_2FC
C00526	Deoxyuridine	-5.015
C03172	S-Methyl-L-methionine	4.64
C06327	Chelirubine	4.625

Fig. 10. The relevant pathway-compound network in the host response to the infection. Compounds in the list are arranged in order of the mean $|log_2FC|$ values from two comparisons.

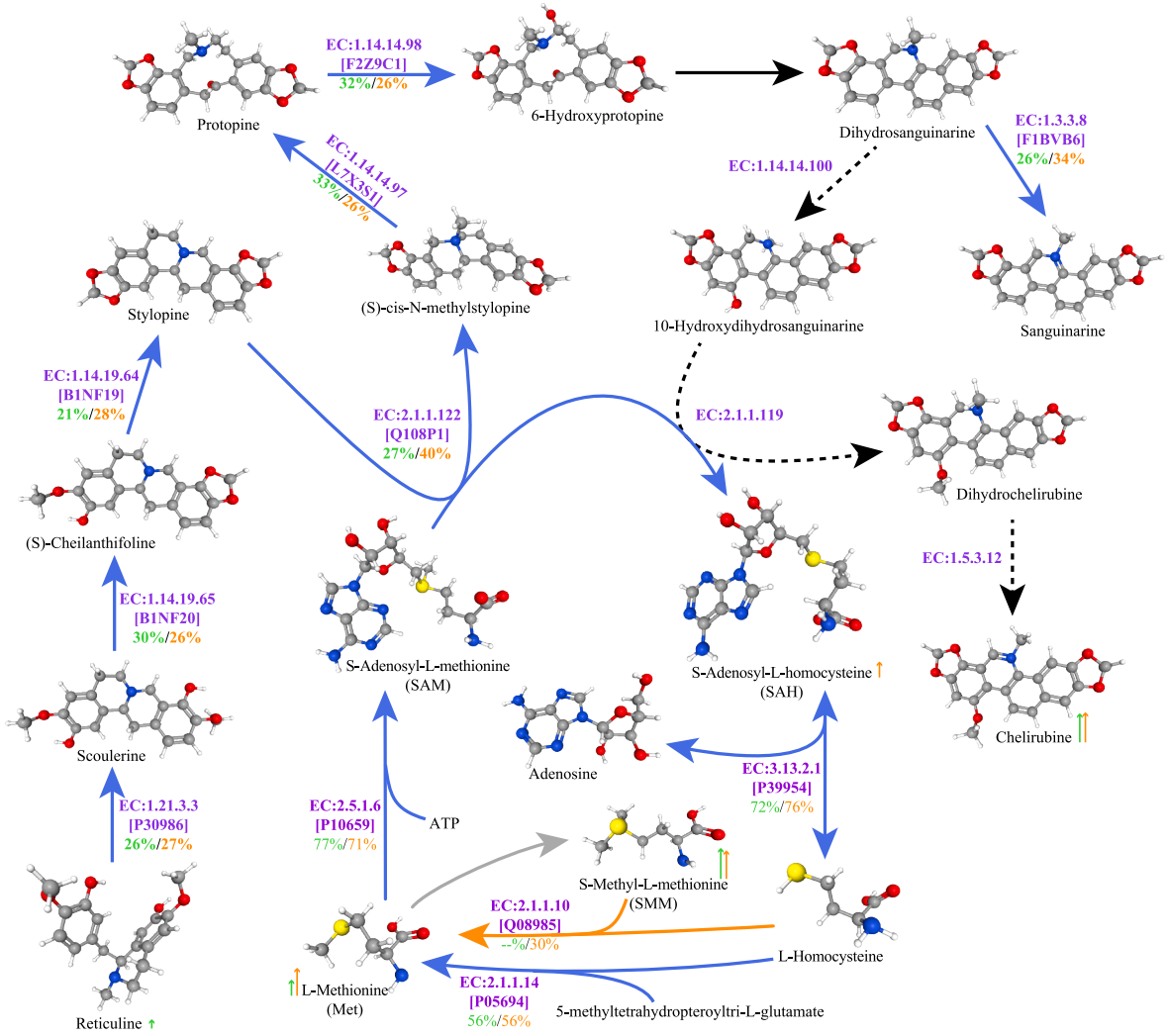

Fig. 11. Reference biosynthesis of sanguinarine and its relevant pathways in the host response to the infection. Proteins catalyzing each reaction are displayed in purple between the two compounds, with corresponding enzyme codes or names shown above and reference UniProtKB entries in the bracket. The similarity of homologs in the pathogen and host genome to protein sequences of reference enzymes is displayed in lime green and dark orange color below the information on enzymes. Arrows between each two compounds indicate the direction of reactions, with their occurrence indicated in royal blue (both pathogen and host), dark orange (only host), grey (neither pathogen nor host), and black (no information) color. Arrows next to the compound indicate the abundance variation in DC (lime green) and HC (dark orange). (For interpretation of the references to color in this figure legend, the reader is referred to the Web version of this article.)

processes of pathogen infection and host response. This underscores the profound significance of methyl group turnover in this battle. Additionally, the consumption of *C. militaris* contaminated by *Ca. cordycipiticola* is strongly discouraged due to the high risk of containing lethal toxins. These findings will significantly enhance our understanding of the pathogen-host interaction, potentially laying the theoretical foundation for more effective prevention and control measures in the future.

CRediT authorship contribution statement

Li Lu: Methodology, Data curation. **Mahesh C.A. Galappaththi:** Writing – review & editing, Conceptualization. **Nimesha M. Patabendige:** Writing – review & editing, Conceptualization. **Yu-Zhe Feng:** Writing – review & editing. **Tian Yang:** Writing – review & editing. **Samantha C. Karunarathna:** Writing – original draft. **Jiang-Tao Xie:** Methodology. **Eleni Gentekaki:** Writing – review & editing. **Sylvie Rapior:** Writing – review & editing. **Esteban Charria-Girón:** Writing – review & editing. **Marc Stadler:** Writing – review & editing. **Wei-Feng Ding:** Writing – review & editing. **Feng-Hua Tian:** Writing – review & editing. **Xiang-Yu Zeng:** Writing – original draft.

Data availability

Data will be made available on request.

Funding

This research was supported by Guizhou Provincial Basic Research Program (Natural Science) ZK[2023] general 087; National Natural Science Foundation of China [No. 32260044]; National Natural Science Foundation of China [No. 32260004]; Guizhou Province Edible Mushroom Industry Technology System (GZMARS-SYJ-2024-2026); Natural Science Special Research Fund of Guizhou University [Special Post 2021 (25)]; China Scholarship Council [[2021]15 no. 202108520071]; Yunnan Technological Innovation Talent Training Object Project [202305AD160037]; HZI POF IV Cooperativity and Creativity Project Call.

Declaration of competing interest

The authors declare that they have no known competing financial interests or personal relationships that could have appeared to influence the work reported in this paper.

Acknowledgements

The authors would like to thank Guizhou Houyuan Agricultural Development Co., Ltd., Guizhou, China for offering samples of *C. militaris* and Wei-Zhen Wang for his valuable advice on the analysis of functional compounds. Li Lu thanks Mae Fah Luang University for the award of a fee-less scholarship and the thesis writing grant. Samantha C. Karunarathna thanks Yunnan Revitalization Talents Support Plan (High-End Foreign Experts Program), and the Key Laboratory of Yunnan Provincial Department of Education of the Deep-Time Evolution on Biodiversity from the Origin of the Pearl River.

Appendix A. Supplementary data

Supplementary data to this article can be found online at https://doi.org/10.1016/j.funbio.2025.101561.

References

Aguileta, G., Hood, M.E., Refregier, G., Giraud, T., 2009. Genome evolution in plant pathogenic and symbiotic fungi. Adv. Bot. Res. 49, 151–193. https://doi.org/10.1016/S0065-2296(08)00603-4.

Alonso-Jauregui, M., López de Cerain, A., Azqueta, A., Rodriguez-Garraus, A., Gil, A.G., González-Peñas, E., Vettorazzi, A., 2023. In vivo genotoxicity and toxicity assessment of sterigmatocystin individually and in mixture with aflatoxin B1. Toxins 15, 491. https://doi.org/10.3390/toxins15080491.

Ando, S., Sato, Y., Shigemori, H., Shimizu, T., Okada, K., Yamane, H., Jikumaru, Y., Kamiya, Y., Yamada, K., Akimoto-Tomiyama, C., Tanabe, S., Nishizawa, Y., Minami, E., 2010. Identification and characterization of 2′-deoxyuridine from the supernatant of conidial suspensions of rice blast fungus as an infection-promoting factor in rice plants. Mol. Plant Microbe Interact. 24, 519–532. https://doi.org/10.1094/MPMI-07-10-0172.

Armenta-Medina, D., Segovia, L., Perez-Rueda, E., 2014. Comparative genomics of nucleotide metabolism: a tour to the past of the three cellular domains of life. BMC Genom. 15, 800. https://doi.org/10.1186/1471-2164-15-800.

Bradshaw, R.E., Jin, H., Morgan, B.S., Schwelm, A., Teddy, O.R., Young, C.A., Zhang, S., 2006. A polyketide synthase gene required for biosynthesis of the aflatoxin-like toxin, dothistromin. Mycopathologia 161, 283–294. https://doi.org/10.1007/s11046-006-0240-5.

Chatree, S., Thongmaen, N., Tantivejkul, K., Sitticharoon, C., Vucenik, I., 2020. Role of inositols and inositol phosphates in energy metabolism. Molecules 25, 5079. https://doi.org/10.3390/molecules25215079.

Chen, L.H., Lin, C.H., Chung, K.R., 2013. A nonribosomal peptide synthetase mediates siderophore production and virulence in the citrus fungal pathogen *Alternaria alternata*. Mol. Plant Pathol. 14, 497–505. https://doi.org/10.1111/mpp.12021.

Chen, Y., Wu, Y., Liu, L., Feng, J., Zhang, T., Qin, S., Zhao, X., Wang, C., Li, D., Han, W., 2019. Study of the whole genome, methylome and transcriptome of *Cordyceps militaris*. Sci. Rep. 9, 898. https://doi.org/10.1038/s41598-018-38021-4.

Cheng, J.-T., Cao, F., Chen, X.-A., Li, Y.-Q., Mao, X.-M., 2020. Genomic and transcriptomic survey of an endophytic fungus *Calcarisporium arbuscula* NRRL 3705 and potential overview of its secondary metabolites. BMC Genom. 21, 424. https://doi.org/10.1186/s12864-020-06813-6.

Cheng, J.-T., Yu, J.-H., Sun, C.-F., Cao, F., Ying, Y.-M., Zhan, Z.-J., Li, W.-J., Chen, X.-A., Zhao, Q.-W., Li, Y.-Q., Gan, L.-S., Mao, X.-M., 2021. A cell factory of a fungicolous fungus *Calcarisporium arbuscula* for efficient production of natural products. ACS Synth. Biol. 10, 698–706. https://doi.org/10.1021/acssynbio.0c00371.

Croaker, A., Davis, A., Carroll, A., et al., 2022. Understanding of black salve toxicity by multi-compound cytotoxicity assays. BMC Complement Med. Ther. 22, 247. https://doi.org/10.1186/s12906-022-03721-y.

Cui, G., Bi, X., Lu, S., Jiang, Z., Deng, Y., 2023. A genetically engineered *Escherichia coli* for potential utilization in fungal smut disease control. Microorganisms 11, 1564. https://doi.org/10.3390/microorganisms11061564.

Cui, J., Gizzi, A., Stivers, J.T., 2019. Deoxyuridine in DNA has an inhibitory and promutagenic effect on RNA transcription by diverse RNA polymerases. Nucleic Acids Res. 47, 4153–4168. https://doi.org/10.1093/nar/gkz183.

Dai, C., Tian, E., Hao, Z., Tang, S., Wang, Z., Sharma, G., Jiang, H., Shen, J., 2022. Aflatoxin B1 toxicity and protective effects of curcumin: molecular mechanisms and clinical implications. Antioxidants 11, 2031. https://doi.org/10.3390/antiox11102031.

Díaz Nieto, C.H., Granero, A.M., Zon, M.A., Fernández, H., 2018. Sterigmatocystin: a mycotoxin to be seriously considered. Food Chem. Toxicol. 118, 460–470. https://doi.org/10.1016/j.fct.2018.05.057.

Domínguez-Santos, R., Kosalková, K., Sánchez-Orejas, I.-C., Barreiro, C., Pérez-Pertejo, Y., Reguera, R.M., Balaña-Fouce, R., García-Estrada, C., 2022. Characterization of the gene encoding *S*-adenosyl-L-methionine (AdoMet) synthetase in *Penicillium chrysogenum*; Role in secondary metabolism and penicillin production. Microorganisms 10, 78. https://doi.org/10.3390/microorganisms10010078.

Dunn, W.B., Broadhurst, D., Begley, P., Zelena, E., Francis-McIntyre, S., Anderson, N., Brown, M., Knowles, J.D., Halsall, A., Haselden, J.N., 2011. Procedures for large-scale metabolic profiling of serum and plasma using gas chromatography and liquid chromatography coupled to mass spectrometry. Nat. Protoc. 6, 1060–1083. https://doi.org/10.1038/nprot.2011.335.

Eckmann, L., Rudolf, M.T., Ptasznik, A., Schultz, C., Jiang, T., Wolfson, N., Tsien, R., Fierer, J., Shears, S.B., Kagnoff, M.F., 1997. D-myo-Inositol 1,4,5,6-tetrakisphosphate produced in human intestinal epithelial cells in response to *Salmonella* invasion inhibits phosphoinositide 3-kinase signaling pathways. Proc. Natl. Acad. Sci. 94, 14456–14460. https://doi.org/10.1073/pnas.94.26.14456.

Feng, J., Wu, J., Dai, N., Lin, S., Xu, H.H., Deng, Z., He, X., 2013. Discovery and characterization of BlsE, a radical *S*-adenosyl-L-methionine decarboxylase involved in the blasticidin S biosynthetic pathway. PLoS One 8, e68545. https://doi.org/10.1371/journal.pone.0068545.

Fiehn, O., 2002. Metabolomics – the link between genotypes and phenotypes. Plant Mol. Biol. 48, 155–171. https://doi.org/10.1007/978-94-010-0448-0_11.

Fodorpataki, L., Molnar, K., Tompa, B., Plugaru, S.R.C., 2019. Priming with vitamin U enhances cold tolerance of Lettuce (*Lactuca sativa* L.). Not. Bot. Horti. Agrobo. 47, 592–598. https://doi.org/10.15835/nbha47311433.

Gannett, C., Tiller, K., Briganti, A.J., Brown, A.M., Weger-Lucarelli, J., Lowell, A.N., 2024. Forgotten natural products: semisynthetic development of Blasticidin S as an antibiotic lead. ACS Med. Chem. Lett. 15, 362–368. https://doi.org/10.1021/acsmedchemlett.3c00527.

Garavito, M.F., Narváez-Ortiz, H.Y., Zimmermann, B.H., 2015. Pyrimidine metabolism: dynamic and versatile pathways in pathogens and cellular development. J Genet. Genomics 42, 195–205. https://doi.org/10.1016/j.jgg.2015.04.004.

Geng, Q., Hu, J., Xu, P., Sun, T., Qiu, H., Wang, S., Song, F., Shen, L., Li, Y., Liu, M., Peng, X., Tian, J., Yang, K., 2024. The autophagy-related protein ATG8 orchestrates asexual development and AFB1 biosynthesis in *Aspergillus flavus*. J. Fungi (Basel). 10, 349. https://doi.org/10.3390/jof10050349.

Ghoshal, S., Tyagi, R., Zhu, Q., Chakraborty, A., 2016. Inositol hexakisphosphate kinase-1 interacts with perilipin1 to modulate lipolysis. Int. J. Biochem. Cell Biol. 78, 149–155. https://doi.org/10.1016/j.biocel.2016.06.018.

Guo, Y., Zhao, L., Ma, Q., Ji, C., 2021. Novel strategies for degradation of aflatoxins in food and feed: a review. Food Res. Int. 140, 109878. https://doi.org/10.1016/j.foodres.2020.109878.

Hof, H., Kupfahl, C., 2009. Gliotoxin in *Aspergillus fumigatus*: an example that mycotoxins are potential virulence factors. Mycotoxin Res. 25, 123–131. https://doi.org/10.1007/s12550-009-0020-4.

Hu, Z., Hu, H., Hu, Z., Zhong, X., Guan, Y., Zhao, Y., Wang, L., Ye, L., Ming, L., Rajoka, M. S.R., 2022. Sanguinarine, isolated from *Macleaya cordata*, exhibits potent antifungal efficacy against *Candida albicans* through inhibiting ergosterol synthesis. Front. Microbiol. 13, 908461. https://doi.org/10.3389/fmicb.2022.908461.

Jiao, X., Fu, X., Li, Q., Bu, J., Liu, X., Savolainen, O., Huang, L., Guo, J., Nielsen, J., Chen, Y., 2024. De novo production of protoberberine and benzophenanthridine alkaloids through metabolic engineering of yeast. Nat. Commun. 15, 8759. https://doi.org/10.1038/s41467-024-53045-3.

Kämper, J., Kahmann, R., Bölker, M., Ma, L.-J., Brefort, T., Saville, B.J., Banuett, F., Kronstad, J.W., Gold, S.E., Müller, O., et al., 2006. Insights from the genome of the biotrophic fungal plant pathogen *Ustilago maydis*. Nature 444, 97–101. https://doi.org/10.1038/nature05248.

Karlsson, M., Durling, M.B., Choi, J., Kosawang, C., Lackner, G., Tzelepis, G.D., Nygren, K., Dubey, M.K., Kamou, N., Levasseur, A., 2015. Insights on the evolution of mycoparasitism from the genome of *Clonostachys rosea*. Genome Biol. Evol. 7, 465–480. https://doi.org/10.1093/gbe/evu292.

Kawalleck, P., Plesch, G., Hahlbrock, K., Somssich, I.E., 1992. Induction by fungal elicitor of *S*-adenosyl-L-methionine synthetase and *S*-adenosyl-L-homocysteine hydrolase mRNAs in cultured cells and leaves of *Petroselinum crispum*. Proc. Natl. Acad. Sci. 89, 4713–4717. https://doi.org/10.1073/pnas.89.10.4713.

Kelman, M.J., Miller, J.D., Renaud, J.B., Baskova, D., Sumarah, M.W., 2024. A multi-year study of mycotoxin co-occurrence in wheat and corn grown in Ontario, Canada. Toxins 16, 372. https://doi.org/10.3390/toxins16080372.

Kocsis, M.G., Ranocha, P., Gage, D.A., Simon, E.S., Rhodes, D., Peel, G.J., Mellema, S., Saito, K., Awazuhara, M., Li, C., Meeley, R.B., Tarczynski, M.C., Wagner, C., Hanson, A.D., 2003. Insertional inactivation of the methionine *S*-methyltransferase gene eliminates the *S*-methylmethionine cycle and increases the methylation ratio. Plant Physiol 131, 1808–1815. https://doi.org/10.1104/pp.102.018846.

Li, N., Wu, Y.-X., Zhang, Y.-D., Wang, S.-R., Zhang, G.-C., Yang, J., 2023. Phytic acid is a new substitutable plant-derived antifungal agent for the seedling blight of *Pinus sylvestris* var. *mongolica* caused by *Fusarium oxysporum*. Pestic. Biochem. Physiol. 191, 105341. https://doi.org/10.1016/j.pestbp.2023.105341.

Liu, L., Ji, X., Li, Y., Ji, W., Mo, T., Ding, W., Zhang, Q., 2017. A mechanistic study of the non-oxidative decarboxylation catalyzed by the radical *S*-adenosyl-l-methionine enzyme BlsE involved in blasticidin S biosynthesis. Chem. Comm. 53, 8952–8955. https://doi.org/10.1039/C7CC04286H.

Liu, Q., Dong, C., 2023. Dual transcriptomics reveals interspecific interactions between the mycoparasite *Calcarisporium cordycipiticola* and its host *Cordyceps militaris*. Microbiol. Spectr. 11, e0480004822. https://doi.org/10.1128/spectrum.04800-22.

Liu, Q., Xu, Y., Zhang, X., Li, K., Li, X., Wang, F., Xu, F., Dong, C., 2021. Infection process and genome assembly provide insights into the pathogenic mechanism of destructive mycoparasite *Calcarisporium cordycipiticola* with host specificity. J. Fungi 7, 918. https://doi.org/10.3390/jof7110918.

Ludmerszki, E., Almási, A., Rácz, I., Szigeti, Z., Solti, Á., Oláh, C., Rudnóy, S., 2015. *S*-methylmethionine contributes to enhanced defense against *Maize dwarf mosaic virus* infection in maize. Braz. J. Biol. 38, 771–782. https://doi.org/10.1007/s40415-015-0195-1.

Martins, S.J., Faria, A.F., Pedroso, M.P., Cunha, M.G., Rocha, M.R., Medeiros, F.H.V., 2019. Microbial volatiles organic compounds control anthracnose (*Colletotrichum lindemuthianum*) in common bean (*Phaseolus vulgaris* L.). Biol. Control 131, 36–42. https://doi.org/10.1016/j.biocontrol.2019.01.003.

Matich, E.K., Chavez Soria, N.G., Aga, D.S., Atilla-Gokcumen, G.E., 2019. Applications of metabolomics in assessing ecological effects of emerging contaminants and pollutants on plants. J. Hazard Mater. 373, 527–535. https://doi.org/10.1016/j.jhazmat.2019.02.084.

Miller, D., Xu, H., White, R.H., 2015. *S*-Inosyl-L-homocysteine hydrolase, a novel enzyme involved in *S*-adenosyl-L-methionine recycling. J. Bacteriol. 197, 2284–2291. https://doi.org/10.1128/JB.00080-15.

NRCC, 1985. *Mycotoxins: a Canadian perspective*. National research Council of Canada. Associate Committee on Scientific Criteria for Environmental Quality (22848), 196. https://doi.org/10.4224/40003422.

Ogihara, S., Komatsu, T., Itoh, Y., Miyake, Y., Suzuki, T., Yanagi, K., Kimura, Y., Ueno, T., Hanaoka, K., Kojima, H., Okabe, T., Nagano, T., Urano, Y., 2020. Metabolic-pathway-oriented screening targeting *S*-Adenosyl-l-methionine reveals the epigenetic remodeling activities of naturally occurring catechols. J. Am. Chem. Soc. 142, 21–26. https://doi.org/10.1021/jacs.9b08698.

Omar, S.S., Haddad, M.A., Parisi, S., 2020. Validation of HPLC and enzyme-linked immunosorbent assay (ELISA) techniques for detection and quantification of aflatoxins in different food samples. Foods 9, 661. https://doi.org/10.3390/foods9050661.

Peng, M., Li, C.Y., Chen, X.L., Williams, B.T., Li, K., Gao, Y.N., Wang, P., Wang, N., Gao, C., Zhang, S., Schoelmerich, M.C., Banfield, J.F., Miller, J.B., Le Brun, N.E., Todd, J.D., Zhang, Y.Z., 2022. Insights into methionine S-methylation in diverse organisms. Nat. Commun. 13, 2947. https://doi.org/10.1038/s41467-022-30491-5.

Rossman, A.Y., 1996. Morphological and molecular perspectives on systematics of the Hypocreales. Mycologia 88, 1–19. https://doi.org/10.1080/00275514.1996.12026620.

Rushing, B.R., Selim, M.I., 2019. Aflatoxin B1: a review on metabolism, toxicity, occurrence in food, occupational exposure, and detoxification methods. Food Chem. Toxicol. 124, 81–100. https://doi.org/10.1016/j.fct.2018.11.047.

Sahu, A., Verma, R., Gupta, U., Kashyap, S., Sanyal, I., 2024. An overview of targeted genome editing strategies for reducing the biosynthesis of phytic acid: an anti-nutrient in crop plants. Mol. Biotechnol. 66, 11–25. https://doi.org/10.1007/s12033-023-00722-1.

Saint-Macary, M.E., Barbisan, C., Gagey, M.J., Frelin, O., Beffa, R., Lebrun, M.H., Droux, M., 2015. Methionine biosynthesis is essential for infection in the rice blast fungus *Magnaporthe oryzae*. PLoS One 10, e0111108. https://doi.org/10.1371/journal.pone.0111108.

Sauer, K., Cooke, M.P., 2010. Regulation of immune cell development through soluble inositol-1,3,4,5-tetrakisphosphate. Nat. Rev. Immunol. 10, 257–271. https://doi.org/10.1038/nri2745.

Severn-Ellis, A.A., Schoeman, M.H., Bayer, P.E., Hane, J.K., Rees, D.J.G., Edwards, D., Batley, J., 2022. Genome Analysis of the broad host range necrotroph *Nalanthamala psidii* highlights genes associated with virulence. Front. Plant Sci. 13, 811152. https://doi.org/10.3389/fpls.2022.811152.

Shank, R.A., Foroud, N.A., Hazendonk, P., Eudes, F., Blackwell, B.A., 2011. Current and future experimental strategies for structural analysis of trichothecene mycotoxins — a prospectus. Toxins 3, 1518–1553. https://doi.org/10.3390/toxins3121518.

Singh, N., Sharma, B., 2018. Toxicological effects of berberine and sanguinarine. Front. Mol. Biosci. 5, 21. https://doi.org/10.3389/fmolb.2018.00021.

Slade, L., Chalker, J., Kuksal, N., Young, A., Gardiner, D., Mailloux, R.J., 2017. Examination of the superoxide/hydrogen peroxide forming and quenching potential of mouse liver mitochondria. Biochim. Biophys. Acta - Gen. Subj. 1861, 1960–1969. https://doi.org/10.1016/j.bbagen.2017.05.010.

Sun, J.Z., Dong, C.H., Liu, X.Z., Liu, J.K., Hyde, K.D., 2016. *Calcarisporium cordycipiticola* sp. nov., an important fungal pathogen of *Cordyceps militaris*. Phytotaxa 268, 135–144. https://doi.org/10.11646/phytotaxa.268.2.4.

Szabó, R.T., Kovács-Weber, M., Balogh, K.M., Mézes, M., Kovács, B., 2024. Effect of aflatoxin B1 and sterigmatocystin on DNA repair genes in common carp. Aquat. Toxicol. 276, 107076. https://doi.org/10.1016/j.aquatox.2024.107076.

Szegő, D., Kósa, E., Horváth, E., 2007. Role of S-methylmethionine in the plant metabolism. Acta Agron. Hung. 55, 491–508. https://doi.org/10.1556/AAgr.55.2007.4.9.

Tahir, N.I., Hussain, S., Javed, M., Rehman, H., Shahzady, T.G., Parveen, B., Ali, K.G., 2018. Nature of aflatoxins: their extraction, analysis, and control. J. Food Saf. 38, e12561. https://doi.org/10.1111/jfs.12561.

Thévenot, E.A., Roux, A., Xu, Y., Ezan, E., Junot, C., 2015. Analysis of the human adult urinary metabolome variations with age, body mass index, and gender by implementing a comprehensive workflow for univariate and OPLS statistical analyses. J. Proteome Res. 14, 3322–3335. https://doi.org/10.1021/acs.jproteome.5b00354.

Troyanskaya, O., Cantor, M., Sherlock, G., Brown, P., Hastie, T., Tibshirani, R., Botstein, D., Altman, R.B., 2001. Missing value estimation methods for DNA microarrays. Bioinformatics 17, 520–525. https://doi.org/10.1093/bioinformatics/17.6.520.

Urbaniak, M., Stępień, Ł., Uhlig, S., 2019. Evidence for naturally produced beauvericins containing N-methyl-tyrosine in Hypocreales fungi. Toxins 11, 182. https://doi.org/10.3390/toxins11030182.

van den Belt, M., Gilchrist, C., Booth, T.J., Chooi, Y.-H., Medema, M.H., Alanjary, M., 2023. CAGECAT: the CompArative GEne Cluster Analysis Toolbox for rapid search and visualisation of homologous gene clusters. BMC Bioinform 24, 181. https://doi.org/10.1186/s12859-023-05311-2.

von Döhren, H., 2004. Biochemistry and general genetics of nonribosomal peptide synthetases in fungi. Adv. Biochem. Engin./Biotechnol. 88, 217–264. https://doi.org/10.1007/b99262.

Wang, T., Suzuki, K., Kakisaka, K., Onodera, M., Sawara, K., Takikawa, Y., 2019. L-carnitine prevents ammonia-induced cytotoxicity and disturbances in intracellular amino acid levels in human astrocytes. J. Gastroenterol. Hepatol. 34, 1249–1255. https://doi.org/10.1111/jgh.14497.

Wu, Y., Adeel, M.M., Xia, D., Sancar, A., Li, W., 2024. Nucleotide excision repair of aflatoxin-induced DNA damage within the 3D human genome organization. Nucleic Acids Res. 52, 11704–11719. https://doi.org/10.1093/nar/gkae755.

Xu, M., Guo, J., Li, T., Zhang, C., Peng, X., Xing, K., Qin, S., 2021. Antibiotic effects of volatiles produced by *Bacillus tequilensis* XK29 against the black spot disease caused by *Ceratocystis fimbriata* in postharvest sweet potato. J. Agric. Food Chem. 69, 13045–13054. https://doi.org/10.1021/acs.jafc.1c04585.

Yang, X., Wang, X., Gao, D., Zhang, Y., Chen, X., Xia, Q., Jin, M., Sun, C., He, Q., Wang, R., Liu, K., 2021. Developmental toxicity caused by sanguinarine in zebrafish embryos via regulating oxidative stress, apoptosis and wnt pathways. Toxicol. Lett. 350, 71–80. https://doi.org/10.1016/j.toxlet.2021.07.001.

Yuen, K.-Y., Pascal, G., Wong, S.S.Y., Glaser, P., Woo, P.C.Y., Kunst, F., Cai, J.J., Cheung, E.Y.L., Médigue, C., Danchin, A., 2003. Exploring the *Penicillium marneffei* genome. Arch. Microbiol. 179, 339–353. https://doi.org/10.1007/s00203-003-0533-8.

Zhang, K., Banerjee, K., 2020. A review: sample preparation and chromatographic technologies for detection of aflatoxins in foods. Toxins 12, 539. https://doi.org/10.3390/toxins12090539.

Zhang, L., Fasoyin, O.E., Molnár, I., Xu, Y., 2020. Secondary metabolites from hypocrealean entomopathogenic fungi: novel bioactive compounds. Nat. Prod. Rep. 37, 1181–1206. https://doi.org/10.1039/C9NP00065H.

Zhao, Z.-M., Shang, X.-F., Lawoe, R.K., Liu, Y.-Q., Zhou, R., Sun, Y., Yan, Y.-F., Li, J.-C., Yang, G.-Z., Yang, C.-J., 2019. Anti-phytopathogenic activity and the possible

mechanisms of action of isoquinoline alkaloid sanguinarine. Pestic. Biochem. Physiol. 159, 51–58. https://doi.org/10.1016/j.pestbp.2019.05.015.
Zheng, P., Xia, Y., Xiao, G., Xiong, C., Hu, X., Zhang, S., Zheng, H., Huang, Y., Zhou, Y., Wang, S., 2011. Genome sequence of the insect pathogenic fungus *Cordyceps militaris*, a valued traditional Chinese medicine. Genome Biol. 12, R116. https://doi.org/10.1186/gb-2011-12-11-r116.
Zingales, V., Fernández-Franzón, M., Ruiz, M.-J., 2020. Sterigmatocystin: occurrence, toxicity and molecular mechanisms of action – a review. Food Chem. Toxicol. 146, 111802. https://doi.org/10.1016/j.fct.2020.111802.
Zingales, V., Esposito, M.R., Quagliata, M., Cimetta, E., Ruiz, M.-J., 2024. Cytotoxic effects induced by combined exposure to the mycotoxins sterigmatocystin, ochratoxin A and patulin on human tumour and healthy 3D spheroids. Food Chem. Toxicol. 192, 114951. https://doi.org/10.1016/j.fct.2024.114951.